

On the asymptotic behaviour of shells of revolution in free vibration

Edoardo Artioli · Lourenco Beirão da Veiga ·
Harri Hakula · Carlo Lovadina

Received: date / Accepted: date

Abstract We consider the free vibration problem of thin shells of revolution of constant type of geometry, focusing on the asymptotic behaviour of the lowest eigenfrequency, as the thickness tends to zero. Numerical experiments are computed using two discretization methods, collocation and finite elements, each corresponding to a different shell model. Our results are in agreement with theoretical results obtained using interpolation theory and cited in literature.

Keywords Shell models, Free vibrations, Finite Element Method, Collocation Method, Interpolation Theory.

Introduction

In this paper we study the free vibration problem of thin shells of revolution of constant type of geometry, focusing on the asymptotic behaviour of the lowest eigenfrequency, as the thickness tends to zero. By constant type of geometry we mean that the sign of the Gaussian curvature (see [14], for instance) does not change. In association with the lowest eigenfrequency, we also investigate on the behaviour of some interesting quantities, namely, the ratio of bending strain energy over the total energy, and the wave number.

F. Artioli
Dip. di Ingegneria Civile, Università di Roma "Tor Vergata", Via del Politecnico 1, I-00133 Roma, Italy
and I.M.A.T.I. - C.N.R., Via Ferrata 1, I-27100 Pavia, Italy
E-mail: artioli@imati.cnr.it

L. Beirão da Veiga
Dip. di Matematica, Università di Milano, Via Saldini 50, I-20133 Milano, Italy
and I.M.A.T.I. - C.N.R., Via Ferrata 1, I-27100 Pavia, Italy
E-mail: Lourenco.Beirao@mat.unimi.it

C. Lovadina (Corresponding Author)
Dip. di Matematica, Università di Pavia, Via Ferrata 1, I-27100 Pavia, Italy
and I.M.A.T.I. - C.N.R., Via Ferrata 1, I-27100 Pavia, Italy
E-mail: carlo.lovadina@unipv.it

H. Hakula
Institute of Mathematics, Helsinki University of Technology, P.O.Box 1100, FI-02015 TKK, Finland
E-mail: Harri.Hakula@tkk.fi

In the well-established asymptotic analysis, shell problems can be divided in two categories: *inhibited pure bending* shells or *non-inhibited pure bending* shells (see [18] and [19], for example). For the case corresponding to a *non-inhibited pure bending shell*, the asymptotic behaviour of the lowest eigenfrequency is well-known (cf. [20]). On the contrary, *inhibited pure bending* shells exhibit a wide variety of different situations, which have been recently studied in [2,5]. Here we are concerned with clamped support only, which induces this latter more complex situation.

The plan of the paper is as follows. In Section 1 we formulate the shell eigenvalue problem to be studied. Both the test problems and the prior theoretical results are given there. In Section 2 we describe our two discretization procedures: Naghdi model with the finite element method (FEM) and Kirchhoff-Love model with the collocation model. The obtained numerical results are summarized in Section 3. For both discretizations we get excellent agreement with theoretical predictions. We remark that, due to the particular shell geometries and boundary conditions we consider, the computational problems to be solved are essentially *one-dimensional*. Therefore, numerical locking can be efficiently alleviated by using high-order methods and sufficiently fine meshes. It is evident that different situations require the approximation of *two-dimensional* PDE problems, for which numerical locking phenomena represent a crucial issue. Conclusions are drawn in Section 3.3. Also, in the Appendix 4 we examine a well-known challenging problem – the so-called *monster shell* (see [12]) – in the eigenvalue setting.

1 Problem presentation

We consider two different 2D shell models: the Naghdi or Reissner-Mindlin model and the Kirchhoff-Love model. The two models under consideration are asymptotically equivalent and can be presented in a unified way.

In essence, assuming a time harmonic displacement field, the free vibration problem for a general shell of thickness t leads to the following *eigenvalue* problem

$$\left\{ \begin{array}{l} \text{Find } \mathbf{u}_t \text{ and } \omega_t^2 \in \mathbb{R} \text{ such that} \\ tA_m \mathbf{u}_t + t^3 A_b \mathbf{u}_t = \omega_t^2 M(t) \mathbf{u}_t \\ + \text{ boundary conditions.} \end{array} \right. \quad (1)$$

Above, \mathbf{u}_t represents the shell displacement field, while ω_t^2 represents the square of the eigenfrequency. The differential operators A_m and A_b account for membrane (or membrane/shear) and bending potential energies, respectively and are *independent of t* . Finally, $M(t)$ is the inertia operator, which in this case can be split into the sum $M(t) = tM^l + t^3M^r$, with M^l and M^r *independent of t* . We remark that the well-known Kirchhoff-Love and Naghdi models fall into this framework.

In what follows, it will be useful to consider also the variational formulation of problem (1). Accordingly, we introduce the space V of admissible displacements, and we consider the problem

$$\left\{ \begin{array}{l} \text{Find } (\mathbf{u}_t, \omega_t^2) \in V \times \mathbb{R} \text{ such that} \\ ta_m(\mathbf{u}_t, \mathbf{v}) + t^3 a_b(\mathbf{u}_t, \mathbf{v}) = \omega_t^2 m^t(\mathbf{u}_t, \mathbf{v}) \quad \forall \mathbf{v} \in V, \end{array} \right. \quad (2)$$

where $a_m(\cdot, \cdot)$, $a_b(\cdot, \cdot)$ and $m^t(\cdot, \cdot)$ are the bilinear forms associated with the operators A_m , A_b and $M(t)$, respectively. Obviously, the space V and the three bilinear forms depend on the chosen shell model (see for instance [12]).

Remark 1 In this paper we are interested in the *smallest* eigenvalue of problem (2), still denoted by ω_t^2 , and in particular we focus on the asymptotic behaviour of the function $t \rightarrow \omega_t^2$, as $t \rightarrow 0^+$.

1.1 Physical test problems

We consider a set of shells of revolution, whose midsurfaces are defined as follows. Let $I = [\alpha, \beta] \subset \mathbb{R}$ be a bounded closed interval, and let $f(x) : I \rightarrow \mathbb{R}^+$ be a regular function. The shell midsurface is parametrised by means of the mapping

$$\begin{aligned} \phi : I \times [0, 2\pi] &\longrightarrow \mathbb{R}^3 \\ \phi(x_1, x_2) &= (x_1, f(x_1) \sin x_2, f(x_1) \cos x_2). \end{aligned} \quad (3)$$

Refer to Figure 1 for a pictorial view of the curvilinear coordinates x_1 and x_2 adopted for this description.

In what follows we will refer to the following kinds of shells of revolution, grouped in terms of Gaussian curvature (see for instance [14]), which cover all the fundamental types of mid-surface geometry. All the shells are assumed to be clamped at the boundary.

1 – *Parabolic [Zero Gaussian curvature shells]*. We have

$$f''(x_1) = 0, \quad \forall x_1 \in I \quad (4)$$

2 – *Elliptic [Positive Gaussian curvature shells]*. We have

$$f''(x_1) < 0, \quad \forall x_1 \in I \quad (5)$$

3 – *Hyperbolic [Negative Gaussian curvature shells]*. We have

$$f''(x_1) > 0, \quad \forall x_1 \in I \quad (6)$$

1.2 Theoretical results

We now present some theoretical results on the asymptotic behaviour of the shell eigenvalue problem (2) for the three types of geometry presented above. In particular, we are interested in the three functions:

$$\begin{aligned} t &\longmapsto \omega_t^2; \\ t &\longmapsto R(t, \mathbf{u}_t) := \frac{t^3 a_b(\mathbf{u}_t, \mathbf{u}_t)}{t^3 a_b(\mathbf{u}_t, \mathbf{u}_t) + t a_m(\mathbf{u}_t, \mathbf{u}_t)} = \frac{t^2 a_b(\mathbf{u}_t, \mathbf{u}_t)}{t^2 a_b(\mathbf{u}_t, \mathbf{u}_t) + a_m(\mathbf{u}_t, \mathbf{u}_t)}; \\ t &\longmapsto K_t. \end{aligned} \quad (7)$$

We recall that ω_t^2 represents the smallest eigenvalue, and the corresponding eigenfrequency is ω_t . We note that $R(t, \mathbf{u}_t)$ represents the ratio of bending strain energy over total strain energy, associated with ω_t^2 and a corresponding eigenvector \mathbf{u}_t . Finally, K_t denotes the wave

number associated with the smallest eigenvalue. Since we are only interested in shells of full revolution, K_t is always integer valued, that is, $t \mapsto K_t : \mathbb{R} \rightarrow \mathbb{N} \cup \{0\}$.

We now need to introduce the following notation concerning the behaviour of the function $t \mapsto \omega_t^2$. When we write

$$\omega_t^2 \sim t^\alpha \quad \alpha \in \mathbb{R}, \quad (8)$$

we mean that

$$\forall \varepsilon > 0 \quad : \quad \lim_{t \rightarrow 0^+} \frac{\omega_t^2}{t^{\alpha-\varepsilon}} = 0 \quad \text{and} \quad \lim_{t \rightarrow 0^+} \frac{\omega_t^2}{t^{\alpha+\varepsilon}} = +\infty. \quad (9)$$

Remark 2 $\omega_t^2 \sim t^\alpha$ essentially means that t^α is the *best power of t* which asymptotically fits ω_t^2 . In some sense, we are measuring the behaviour of ω_t^2 by using the scale of the real power functions. We also notice that $\omega_t^2 \sim t^\alpha$ *does not* imply that ω_t^2 behaves *exactly* like t^α . For instance, we have $\omega_t^2 \sim t^\alpha$ for $\omega_t^2 = -t^\alpha \log t$, in accordance with (8)–(9).

For fully clamped shells of revolution, the following results can be established applying the results of [5, 6]; the proof can be found in [2].

1 – *Parabolic [Zero Gaussian curvature shells]*. We have:

$$\omega_t^2 \sim t \quad ; \quad \lim_{t \rightarrow 0^+} R(t, \mathbf{u}_t) = \frac{1}{2}. \quad (10)$$

Therefore, the first eigenfrequency ω_t behaves like $t^{1/2}$ in the sense of Remark 2, and the bending energy associated to the first vibration mode is approximatively half of the total energy, for “small” t .

2 – *Elliptic [Positive Gaussian curvature shells]*.

$$\omega_t^2 \sim t^0 \quad ; \quad \lim_{t \rightarrow 0^+} R(t, \mathbf{u}_t) = 0. \quad (11)$$

Therefore, the first eigenfrequency ω_t behaves like a constant in the sense of Remark 2, and the bending energy associated to the first vibration mode is negligible with respect to the total energy, for “small” t .

3 – *Hyperbolic [Negative Gaussian curvature shells]*.

$$\omega_t^2 \sim t^{2/3} \quad ; \quad \lim_{t \rightarrow 0^+} R(t, \mathbf{u}_t) = \frac{1}{3}. \quad (12)$$

Therefore, the first eigenfrequency ω_t behaves like $t^{1/3}$ in the sense of Remark 2, and the bending energy associated to the first vibration mode is approximatively one third of the total energy, for “small” t .

For the map $t \mapsto K_t$, the only theoretical proof is for the parabolic case (see [7]): $K_t \sim t^{-\frac{1}{4}}$. For the other cases, the rates are deduced numerically from our results, as shown in Section 3.3.

2 Problem discretizations

In this section we present the two discretization procedures we use for the shell analyses. The first scheme is a classical finite element method, while the second one employs a collocation strategy. Although both the methods are based on a 2D shell model, the structure of shells of revolution allows a further dimension reduction. Accordingly, the actual computations will be performed on the basis of the discretization of the corresponding *1D model* which is addressed here below.

2.1 Dimensional reduction by Fourier series decoupling of dependent variables

In order to deal with a one-dimensional problem instead than with a bi-dimensional one, it proves efficient to adopt the following Fourier series expansion of displacements and rotations with respect to the circumferential coordinate x_2 . We are then interested in a solution of the following form:

Displ. component	Naghdi model	Kirchhoff-Love model	
$u(x_1, x_2)$	$\sum_{K \in \mathbb{N}} u^{(K)}(x_1) \cos(Kx_2)$	$\sum_{K \in \mathbb{N}} u^{(K)}(x_1) \cos(Kx_2)$	
$v(x_1, x_2)$	$\sum_{K \in \mathbb{N}} v^{(K)}(x_1) \sin(Kx_2)$	$\sum_{K \in \mathbb{N}} v^{(K)}(x_1) \sin(Kx_2)$	
$w(x_1, x_2)$	$\sum_{K \in \mathbb{N}} w^{(K)}(x_1) \cos(Kx_2)$	$\sum_{K \in \mathbb{N}} w^{(K)}(x_1) \cos(Kx_2)$	(13)
$\theta(x_1, x_2)$	$\sum_{K \in \mathbb{N}} \theta^{(K)}(x_1) \cos(Kx_2)$		
$\psi(x_1, x_2)$	$\sum_{K \in \mathbb{N}} \psi^{(K)}(x_1) \sin(Kx_2)$		

which decouples the displacement field in the two coordinate directions. The above Fourier expansions lead to a (theoretically infinite) series of solution sets, in terms of harmonic amplitudes

$$\begin{aligned} \mathbf{u}^{(K)}(x_1) &= [u^{(K)}, v^{(K)}, w^{(K)}, \theta^{(K)}, \psi^{(K)}]^T && \text{(Naghdi)} \\ \mathbf{u}^{(K)}(x_1) &= [u^{(K)}, v^{(K)}, w^{(K)}]^T && \text{(Kirchhoff-Love)} \end{aligned} \quad (14)$$

which are function of the longitudinal coordinate x_1 and are characterized by the harmonic number K . Each of these solutions can be found by solving a one dimensional eigenvalue problem associated to the parameter K .

2.2 Discretization procedures

2.2.1 Naghdi model with the finite element method

Let the shell midsurface be described by the map ϕ introduced in (3). In the sequel we will need the following geometrical quantities.

$$\begin{aligned} a &= [1 + (f')^2] f^2, \\ a^{11} &= \frac{1}{1 + (f')^2}, \quad a^{22} = \frac{1}{f^2}, \quad a^{12} = a^{21} = 0, \\ b_{11} &= \frac{-f''f}{\sqrt{a}}, \quad b_{22} = \frac{f^2}{\sqrt{a}}, \quad b_{12} = b_{21} = 0, \\ \Gamma_{11}^1 &= \frac{f''f'f^2}{a}, \quad \Gamma_{22}^1 = \frac{-f'f^3}{a}, \quad \Gamma_{12}^2 = \Gamma_{21}^2 = \frac{f'}{f}, \\ \Gamma_{12}^1 &= \Gamma_{21}^1 = \Gamma_{11}^2 = \Gamma_{22}^2 = 0. \end{aligned} \quad (15)$$

For the sake of notational simplicity, the dependence of all the quantities on the coordinate x_1 is omitted. We also notice that a represents the determinant of the metric tensor for the

surface, $b_{\sigma\tau}$ is the curvature tensor and $\Gamma_{\sigma\tau}^\gamma$ are the Christoffel symbols. Finally, we recall that

$$b_\tau^\sigma = a^{\sigma\mu} b_{\mu\tau}. \quad (16)$$

A description of the Naghdi model can be found in [12]. A major feature of the model is that the shell displacements are described by means of the midsurface displacements and the fiber rotations. As a consequence, the unknown \mathbf{u}_t in Section 1 here becomes the five-component function

$$\mathbf{u}_t = [u_t, v_t, w_t, \theta_t, \psi_t]^T \in V^N,$$

where V^N is a suitable space of admissible functions. Since finite elements will be used, we directly present the variational formulation of the model equations for the *one-dimensional* problems ensuing from the decoupling procedure at the beginning of Section 2.1. The bending, membrane, shear and mass bilinear forms for the K -th harmonic number are respectively given by

$$\begin{aligned} a_b^{(K)}(\mathbf{u}, \hat{\mathbf{u}}) &= \frac{\pi}{12} \int_\alpha^\beta C_{\sigma\tau\delta\mu} \chi_{\sigma\tau}^{(K)}(\mathbf{u}) \chi_{\delta\mu}^{(K)}(\hat{\mathbf{u}}) \sqrt{a} dx_1, \\ a_m^{(K)}(\mathbf{u}, \hat{\mathbf{u}}) &= \pi \int_\alpha^\beta C_{\sigma\tau\delta\mu} \gamma_{\sigma\tau}^{(K)}(\mathbf{u}) \gamma_{\delta\mu}^{(K)}(\hat{\mathbf{u}}) \sqrt{a} dx_1, \\ a_s^{(K)}(\mathbf{u}, \hat{\mathbf{u}}) &= \pi \int_\alpha^\beta D_{\sigma\delta} \rho_\sigma^{(K)}(\mathbf{u}) \rho_\delta^{(K)}(\hat{\mathbf{u}}) \sqrt{a} dx_1, \\ m^t(\mathbf{u}, \hat{\mathbf{u}}) &= \pi \int_\alpha^\beta [t(u\hat{u} + v\hat{v} + w\hat{w}) + \frac{t^3}{12}(\theta\hat{\theta} + \psi\hat{\psi})] \sqrt{a} dx_1, \end{aligned} \quad (17)$$

for all $\mathbf{u} = [u, v, w, \theta, \psi]^T \in [H_0^1(I)]^5$ and variations $\hat{\mathbf{u}} = [\hat{u}, \hat{v}, \hat{w}, \hat{\theta}, \hat{\psi}]^T \in [H_0^1(I)]^5$.

The bending, membrane and shear strains are respectively defined as

$$\begin{aligned} \chi_{11}^{(K)}(\mathbf{u}) &= \theta' - \Gamma_{11}^1 \theta - \Gamma_{11}^2 \psi + b_1^2(v' - \Gamma_{21}^1 u - \Gamma_{21}^2 v - b_{21} w) + b_1^1 \gamma_{11}^{(K)}, \\ \chi_{22}^{(K)}(\mathbf{u}) &= K\psi - \Gamma_{22}^1 \theta - \Gamma_{22}^2 \psi + b_2^1(-Ku - \Gamma_{12}^1 u - \Gamma_{12}^2 v - b_{12} w) + b_2^2 \gamma_{22}^{(K)}, \\ \chi_{12}^{(K)}(\mathbf{u}) &= \frac{1}{2}(-K\theta + \psi') - \Gamma_{12}^1 \theta - \Gamma_{12}^2 \psi + \frac{1}{2} b_1^1(-Ku - \Gamma_{12}^1 u - \Gamma_{12}^2 v - b_{12} w) \\ &\quad + \frac{1}{2} b_2^2(v' - \Gamma_{21}^1 u - \Gamma_{21}^2 v - b_{21} w) + \frac{1}{2} b_2^1 \gamma_{11}^{(K)} + \frac{1}{2} b_1^2 \gamma_{22}^{(K)} = \chi_{21}^{(K)}(\mathbf{u}), \\ \gamma_{11}^{(K)}(\mathbf{u}) &= u' - \Gamma_{11}^1 u - \Gamma_{11}^2 v - b_{11} w, \\ \gamma_{22}^{(K)}(\mathbf{u}) &= Kv - \Gamma_{22}^1 u - \Gamma_{22}^2 v - b_{22} w, \\ \gamma_{12}^{(K)}(\mathbf{u}) &= \frac{1}{2}(-Ku + v') - \Gamma_{12}^1 u - \Gamma_{12}^2 v - b_{12} w = \gamma_{21}^{(K)}(\mathbf{u}), \\ \rho_1^{(K)}(\mathbf{u}) &= w' + b_1^1 u + b_1^2 v - \theta, \\ \rho_2^{(K)}(\mathbf{u}) &= -Kw + b_2^1 u + b_2^2 v - \psi. \end{aligned} \quad (18)$$

Furthermore, the fourth order tensor C and the second order tensor D are given by $C_{1111} = 1, C_{2222} = 1, C_{1122} = 2\nu, C_{1212} = (1 - \nu), C_{2121} = (1 - \nu)$, otherwise $C_{\sigma\tau\delta\mu} = 0$ and $D_{11} = D_{22} = \frac{1}{2}(1 - \nu)$, otherwise $D_{\sigma\tau} = 0$.

Therefore, the variational formulation of the one-dimensional eigenvalue problem, associated to the harmonic number K , takes the form

$$\begin{cases} \text{Find } \mathbf{u}^{(K)} = [u^{(K)}, v^{(K)}, w^{(K)}, \theta^{(K)}, \psi^{(K)}]^T \in [H_0^1(I)]^5 \text{ and } \omega_t^{(K)} \in \mathbb{R} \text{ such that} \\ t^3 a_b^{(K)}(\mathbf{u}^{(K)}, \hat{\mathbf{u}}) + t \left(a_m^{(K)}(\mathbf{u}^{(K)}, \hat{\mathbf{u}}) + a_s^{(K)}(\mathbf{u}^{(K)}, \hat{\mathbf{u}}) \right) = (\omega_t^{(K)})^2 m^t(\mathbf{u}^{(K)}, \hat{\mathbf{u}}), \end{cases} \quad (19)$$

for every test function $\hat{\mathbf{u}} = [\hat{u}^{(K)}, \hat{v}^{(K)}, \hat{w}^{(K)}, \hat{\theta}^{(K)}, \hat{\psi}^{(K)}]^T \in [H_0^1(I)]^5$. Note that, for notation convenience, here and in the sequel the dependence of the solution $\mathbf{u}^{(K)}$ on the thickness parameter t is omitted.

The finite-element method used is based on the p -extension of FEM [22]. Let \mathcal{T}_h be a subdivision of I , h being the mesh-size. We set $S_h \subset [H_0^1(I)]^5$ as the space of globally continuous functions, which are piecewise polynomials of degree at most p . Then the discrete problem reads

$$\begin{cases} \text{Find } \mathbf{u}_h^{(K)} = [u_h^{(K)}, v_h^{(K)}, w_h^{(K)}, \theta_h^{(K)}, \psi_h^{(K)}]^T \in S_h \text{ and } \omega_{t,h}^{(K)} \in \mathbb{R} \text{ such that} \\ t^3 a_b^{(K)}(\mathbf{u}_h^{(K)}, \hat{\mathbf{u}}_h) + t \left(a_m^{(K)}(\mathbf{u}_h^{(K)}, \hat{\mathbf{u}}_h) + a_s^{(K)}(\mathbf{u}_h^{(K)}, \hat{\mathbf{u}}_h) \right) = (\omega_{t,h}^{(K)})^2 m^t(\mathbf{u}_h^{(K)}, \hat{\mathbf{u}}_h), \end{cases} \quad (20)$$

for every discrete test function $\hat{\mathbf{u}}_h = [\hat{u}_h^{(K)}, \hat{v}_h^{(K)}, \hat{w}_h^{(K)}, \hat{\theta}_h^{(K)}, \hat{\psi}_h^{(K)}]^T \in S_h$. In the construction of S_h the basis functions are divided into nodal and bubble functions. The node functions are the standard hat-functions

$$N_1(\xi) = \frac{1-\xi}{2}, \quad N_2(\xi) = \frac{1+\xi}{2}, \quad (21)$$

and the bubble functions $N_i(\xi) = \varphi_{i-1}(\xi)$, $i = 3, 4, \dots, p+1$ are defined in terms of the Legendre polynomials P_{j-1}

$$\varphi_j(\xi) = \sqrt{\frac{2j-1}{2}} \int_{-1}^{\xi} P_{j-1}(t) dt, \quad j = 2, 3, \dots \quad (22)$$

2.2.2 The Kirchhoff-Love model with the collocation method

In this section we provide a brief outline of the one-dimensional strong form of the problem under consideration, in the framework of the Kirchhoff-Love hypothesis, and its discretization by a collocation method. Without going into too much detail, it is worth recalling that in this hypothesis transverse shearing strain components are zero. Essentially, this implies rotations to become dependent on midsurface displacements which are the only dependent variables. Equilibrium equations reduce to three. They represent translation dynamic equilibrium along meridional, circumferential and transverse direction, respectively. For more details on the present model, the reader is referred to [13, 17].

Searching for a solution of the type (cf. (14)₂)

$$\mathbf{u}^{(K)}(x_1) = [u^{(K)}(x_1), v^{(K)}(x_1), w^{(K)}(x_1)]$$

the formulation amounts to a set of three linear differential equations for the displacements Fourier amplitudes, plus mixed boundary conditions assigned at $x_1 = \alpha$ and $x_1 = \beta$. Assuming to have clamped boundaries, the following dynamic equilibrium statement holds:

$$\left\{ \begin{array}{l} \text{Find } \mathbf{u}^{(K)} \text{ and } \omega_t^{(K)} \in \mathbf{R} \text{ such that, for any natural number } K, \\ tA_m^{(K)} \mathbf{u}^{(K)} + t^3 A_b^{(K)} \mathbf{u}^{(K)} = \left(\omega_t^{(K)} \right)^2 M(t) \mathbf{u}^{(K)} \quad \forall x_1 \in I \\ \mathbf{u}^{(K)} = \mathbf{0}; \quad \frac{\partial \mathbf{u}^{(K)}}{\partial x_1} = \mathbf{0} \quad \text{for } x_1 = \alpha, \beta \end{array} \right. \quad (23)$$

It is recalled that the dependence of the solution $\mathbf{u}^{(K)}$ on the thickness parameter t is not explicated for notation convenience. The bending and membrane operators $A_m^{(K)}$ and $A_b^{(K)}$, appearing in (23), take into account the three equations of equilibrium which constitute the boundary value problem at hand, for the harmonic amplitudes of displacement. The derivation and the explicit form of the operators $A_m^{(K)}$ and $A_b^{(K)}$ is omitted for brevity, but can be found following for instance the lines in References [23, 1, 21].

We now present the adopted discretization strategy for such a model, based on a Lagrange collocation method [8].

The basic steps of this procedure can be shortly summarized as follows:

- Discretization of the one-dimensional domain I into a finite set of *quadrature points* $\{x_{1i}\}_{i=1, \dots, N}$, such that $x_{11} = \alpha$ and $x_{1N} = \beta$.
- Discretization of the equilibrium operators $A_m^{(K)}$ and $A_b^{(K)}$ through Lagrange interpolants, assuming the solution is a polynomial of degree $(N - 1)$.
- Collocation of governing equations and boundary conditions (23) at internal and boundary quadrature points, respectively.
- Solution of the ensuing discrete (eigenvalue) problem.
- Reconstruction of approximate solution through Lagrange interpolation rule.

For further details on the proposed collocation solution scheme, the Reader is referred, amongst other, to References [1, 10].

Defining $\tilde{\mathbf{u}}_i^{(K)} = \mathbf{u}^{(K)}(x_{1i})$, $i = 1, \dots, N$, one is finally left with the following discrete generalized eigenvalue problem:

$$\left\{ \begin{array}{l} \text{Find } \tilde{\mathbf{u}}_i^{(K)} \text{ and } \tilde{\omega}_t^{(K)} \in \mathbf{R} \text{ such that, for any natural number } K, \\ t\tilde{A}_m^{(K)} \tilde{\mathbf{u}}_i^{(K)} + t^3 \tilde{A}_b^{(K)} \tilde{\mathbf{u}}_i^{(K)} = \left[\tilde{\omega}_t^{(K)} \right]^2 \tilde{M}(t) \tilde{\mathbf{u}}_i^{(K)} \quad \text{for } i = 2, \dots, N - 1 \\ \tilde{\mathbf{u}}_i^{(K)} = \mathbf{0}; \quad \frac{\partial \tilde{\mathbf{u}}_i^{(K)}}{\partial x_1} = \mathbf{0} \quad \text{for } i = 1, N \end{array} \right. \quad (24)$$

The discretized operators $\tilde{A}_m^{(K)}$, $\tilde{A}_b^{(K)}$ and $\tilde{M}(t)$ may be constructed applying the basic steps listed above. For a detailed derivation, see for instance References [1, 3].

2.2.3 Unified notation

Assembling the systems (19) and (24) and partitioning the degrees of freedom of the system within *boundary or nodes* (subscripts b) and *interior or bubbles* (subscript d) ones, leads to the classical form of the generalized eigenvalue problem

$$t \begin{pmatrix} \mathbf{K}_{bb} & \mathbf{K}_{bd} \\ \mathbf{K}_{db} & \mathbf{K}_{dd} \end{pmatrix}_m^{(K)} \begin{pmatrix} \tilde{\mathbf{u}}_b \\ \tilde{\mathbf{u}}_d \end{pmatrix}^{(K)} + t^3 \begin{pmatrix} \mathbf{K}_{bb} & \mathbf{K}_{bd} \\ \mathbf{K}_{db} & \mathbf{K}_{dd} \end{pmatrix}_b^{(K)} \begin{pmatrix} \tilde{\mathbf{u}}_b \\ \tilde{\mathbf{u}}_d \end{pmatrix}^{(K)} = [\tilde{\omega}_t^{(K)}]^2 \begin{pmatrix} \mathbf{M}_{bb}(t) & \mathbf{M}_{bd}(t) \\ \mathbf{M}_{db}(t) & \mathbf{M}_{dd}(t) \end{pmatrix} \begin{pmatrix} \tilde{\mathbf{u}}_b \\ \tilde{\mathbf{u}}_d \end{pmatrix}^{(K)} \quad (25)$$

or, in compact notation

$$(t \mathbf{K}_m^{(K)} + t^3 \mathbf{K}_b^{(K)}) \tilde{\mathbf{u}}^{(K)} = [\tilde{\omega}_t^{(K)}]^2 \mathbf{M}(t) \tilde{\mathbf{u}}^{(K)} \quad (26)$$

which is to be solved for the couples $(\tilde{\mathbf{u}}^{(K)}, \tilde{\omega}^{(K)})$. We also notice that $\mathbf{M}(t)$ has the form $\mathbf{M}(t) = t \mathbf{M}^l$ for the Kirchhoff-Love model, and the form $\mathbf{M}(t) = t \mathbf{M}^l + t^3 \mathbf{M}^r$ for the Naghdi model. Furthermore, we have followed the convention where both bending and shear parts of the Naghdi model are present in $\mathbf{K}_m^{(K)}$.

Using this notation we can define $R(t, \mathbf{u}_t)$ in approximate form as:

$$R(t, \tilde{\mathbf{u}}^{(K)}) = \frac{t^3 [\tilde{\mathbf{u}}^{(K)}]^T \mathbf{K}_b^{(K)} \tilde{\mathbf{u}}^{(K)}}{[\tilde{\mathbf{u}}^{(K)}]^T (t \mathbf{K}_m^{(K)} + t^3 \mathbf{K}_b^{(K)}) \tilde{\mathbf{u}}^{(K)}} = \frac{t^2 [\tilde{\mathbf{u}}^{(K)}]^T \mathbf{K}_b^{(K)} \tilde{\mathbf{u}}^{(K)}}{[\tilde{\mathbf{u}}^{(K)}]^T (\mathbf{K}_m^{(K)} + t^2 \mathbf{K}_b^{(K)}) \tilde{\mathbf{u}}^{(K)}} \quad (27)$$

3 Numerical tests

We illustrate the theoretical results of Section 1.2 on different types of shells of Section 1.1. In Figure 2 we outline the cross sections of our main three test cases and a fourth shell, named “monster shell”, which will be considered later on in the discussion.

For every test geometry, with clamped kinematic constraints, we have computed the values of interest, ω_t^2 , $R(t, \mathbf{u}_t)$, K_t , over a logarithmically distributed set of thicknesses. Every experiment has been performed twice using the two discretizations described in Section 2. The discretizations have been kept fixed over the set of thicknesses:

- *FEM*. In every case 100 elements of constant width with $p = 12$ are used. When clamped boundary conditions are imposed, the resulting generalized eigenvalue problem has 5995 degrees of freedom.
- *Collocation*. The results computed with the collocation method of Section 2.2.2 are obtained by discretizing the domain with 129 quadrature nodes. When clamped boundary conditions are imposed, the resulting generalized eigenvalue problem has 387 degrees of freedom.

The numerical experiments, compared with the related theoretical predictions, have been summarised in Table 1.

3.1 Numerical results on the function $t \mapsto \omega_t^2$

Our numerical results on the asymptotic behaviour of the function $t \mapsto \omega_t^2$ are summarized in Figure 3. The asymptotic behaviour of the shells examined as measured with both

Geometry	Function	Theoretical Prediction	Numerical Results	Comparison
Parabolic $f(x) = 1$ $H = 1$	$t \mapsto \omega_t^2$	$\omega_t^2 \sim t$	Figure 3	Table 2
	$t \mapsto K_t$	$K_t \sim t^{-\frac{1}{4}}$	Figure 6a	
	$t \mapsto R(t, \mathbf{u}_t)$	$\lim_{t \rightarrow 0^+} R(t, \mathbf{u}_t) = \frac{1}{2}$	Figures 4a, 4b	Table 3
Elliptic $f(x) = 1 - \frac{1}{2}x^2$ $H = 0.892668$	$t \mapsto \omega_t^2$	$\omega_t^2 \sim t^0$	Figure 3	Table 2
	$t \mapsto K_t$		Figure 6b	
	$t \mapsto R(t, \mathbf{u}_t)$	$\lim_{t \rightarrow 0^+} R(t, \mathbf{u}_t) = 0$	Figures 4c, 4d	Table 3
Hyperbolic $f(x) = 1 + \frac{1}{2}x^2$ $H = 0.892668$	$t \mapsto \omega_t^2$	$\omega_t^2 \sim t^{2/3}$	Figure 3	Table 2
	$t \mapsto K_t$		Figure 6c	
	$t \mapsto R(t, \mathbf{u}_t)$	$\lim_{t \rightarrow 0^+} R(t, \mathbf{u}_t) = \frac{1}{3}$	Figures 4e, 4f	Table 3

Material constants adopted for all simulations are: $E = 2.069 \times 10^{11}$ MPa, $\mu = 0.3$, $\lambda = 5/6$ and $\rho = 7868$ Kg/m³. The shell geometry is defined in terms of a single parameter $H > 0$, so that the arc length over the interval $[-H, H]$ is 2.

In every experiment clamped boundary conditions have been imposed at both ends $x_1 = -H$ and $x_1 = H$ and results computed for a set of 1601 thicknesses equally spaced on logarithmic scale covering the interval $[10^{-6}, 10^{-2}]$.

Table 1: Guide to numerical experiments.

Geometry	Mean of relative error	STD of relative error	Correlation of values
Parabolic	0.0022	0.0007	1.0000
Elliptic	0.0050	0.0015	1.0000
Hyperbolic	0.0006	0.0009	1.0000

Here we take the FEM-result as the reference. Thus, the relative error is defined as $\text{err} = |\omega_{t,\text{coll}}^2 - \omega_{t,\text{FEM}}^2| / \omega_{t,\text{FEM}}^2$. In the first column we have the mean over the entire span of relative errors per given geometry. In subsequent columns we have the standard deviation of the relative errors and finally the Pearson correlation coefficient of the values of ω_t^2 computed with the two methods.

Table 2: Comparison of $t \mapsto \omega_t^2$.

Geometry	Mean of relative error	STD of relative error	Correlation of values
Parabolic	0.0093	0.0108	0.9952
Elliptic	0.3194	0.9533	0.9649
Hyperbolic	0.0414	0.0406	0.9309

Here we take the FEM-result as the reference. Thus, the relative error is defined as $\text{err} = |R_{\text{coll}}(t, \mathbf{u}_t) - R_{\text{FEM}}(t, \mathbf{u}_t)| / R_{\text{FEM}}(t, \mathbf{u}_t)$. In the first column we have the mean over the entire span of relative errors per given geometry. In subsequent columns we have the standard deviation of the relative errors and finally the Pearson correlation coefficient of the values of $R(t, \mathbf{u}_t)$ computed with the two methods.

Table 3: Comparison of $t \mapsto R(t, \mathbf{u}_t)$.

FEM for the Naghdi model

t	Parabolic	Slopes	Elliptic	Slopes	Hyperbolic	Slopes
10^{-2}	677910.312090		12644780.768739		2830744.389133	
		0.923084		0.129441		0.662881
10^{-3}	80926.028056		9385781.033894		615205.013613	
		0.970509		0.134224		0.663892
10^{-4}	8661.366553		6890428.388354		133391.316884	
		0.992194		0.081613		0.664894
10^{-5}	881.846095		5709958.633337		28855.815479	
		0.997083		0.046465		0.665810
10^{-6}	88.778823		5130597.313294		6229.084873	

Here we give the eigenvalues at specified thickness obtained with the FEM method for the Naghdi model. This is to help confirm the expected slopes in Figure 3. It is clear that in the parabolic case ω_r^2 tends to be $\sim t$, while in the hyperbolic one $\sim t^{2/3}$. In the elliptic case we note that ω_r^2 tends to be $\sim t^0$, but this asymptotic behaviour seems to be reached much slower than in the other two cases.

Table 4: Slopes of $t \mapsto \omega_r^2$.

Collocation for the Kirchhoff-Love model

t	Parabolic	Slopes	Elliptic	Slopes	Hyperbolic	Slopes
10^{-2}	680852.474764		12652595.683286		2835603.432502	
		0.924289		0.132261		0.663322
10^{-3}	81052.006234		9330786.239216		615635.801490	
		0.970414		0.134299		0.664259
10^{-4}	8676.610236		6848880.880890		133372.127086	
		0.991954		0.081299		0.664924
10^{-5}	883.885906		5679633.694851		28849.698698	
		0.996971		0.045936		0.665823
10^{-6}	89.007124		5109567.917717		6227.571443	

Here we give the eigenvalues at specified thickness obtained with the collocation method for the Kirchhoff-Love model. This is to help confirm the expected slopes in Figure 3. It is clear that in the parabolic case ω_r^2 tends to be $\sim t$, while in the hyperbolic one $\sim t^{2/3}$. In the elliptic case we note that ω_r^2 tends to be $\sim t^0$, but this asymptotic behaviour seems to be reached much slower than in the other two cases.

Table 5: Slopes of $t \mapsto \omega_r^2$.

approaches is in agreement with the theory (cf. (10)-(12)). In order to better appreciate the agreement, in Tables 4–5 we plot the progressive interpolated slopes

$$\alpha_i = \log \frac{\omega_r^2|_{t=10^{-i}}}{\omega_r^2|_{t=10^{-i-1}}}, \quad i = 2, 3, \dots, 5,$$

which represent a numerical estimate of the exponent α in the interval $[10^{-i-1}, 10^{-i}]$, see (9). The values α_i clearly converge, for both models, to the theoretical α shown in Table 1.

Finally, the statistical comparison of the two result sets can be found in Table 2. The Pearson correlation coefficient, ranging from -1 to $+1$, reflects the degree of linear relationship between two variables; a correlation of $+1$ indicates a perfect positive linear relationship.

3.2 Numerical results on the function $t \mapsto R(t, \mathbf{u}_t)$

As stated in Section 1.2, we are interested in plotting the asymptotic behavior of the fundamental frequency as the thickness t tends to zero as well as the ratio $R(t, \mathbf{u}_t)$ (cf. (7)), which represents the non dimensional proportion between elastic bending and total potential strain energy associated to the fundamental eigenmode. The statistical comparison of the two result sets can be found in Table 3.

The asymptotic behavior of $R(t, \mathbf{u}_t)$ as measured with both approaches follows the theoretical predictions as $t \rightarrow 0^+$. For relatively thick elliptic shells the difference between the two methods is greatest. Here one should note that this occurs in the full membrane region where $R(t, \mathbf{u}_t)$ is practically zero.

The curious banding profiles of $t \mapsto R(t, \mathbf{u}_t)$ are clear in Figures 4 (and 8 also). Each band corresponds to a given value of K_t .

In Figure 5 we report two-dimensional plots of the local ratio between bending energy and total strain energy density for each considered type of shell at $t = 10^{-3}$. Note that presence of bending dominated regions is usually indicative of possible numerical locking. Due to our one-dimensional approach, our numerical results cannot be used to investigate directly this phenomenon, which is beyond the aims of the present paper.

3.3 Numerical results on the function $t \mapsto K_t$

As one would expect, finding the correct value of K_t is less challenging than getting the ω_t^2 right. Since there is hardly any difference at all between the two sets, we are content to show the results for FEM only in Figure 6. For the same reason, no statistical comparison between the two models is presented.

Note that the missing values of the elliptic plot simply indicate the constant value of ω_t^2 with $K_t = 0$. Our numerical tests suggest that it holds

$$\begin{aligned} K_t &\sim t^{-\frac{1}{4}} && \text{for the parabolic case;} \\ K_t &\sim t^{-\frac{2}{5}} && \text{for the elliptic case;} \\ K_t &\sim t^{-\frac{1}{3}} && \text{for the hyperbolic case.} \end{aligned} \tag{28}$$

Therefore, the slope of the parabolic results is in agreement with the theory, see Table 1. We also notice that in the elliptic case, K_t is probably growing slightly faster than exactly $t^{-2/5}$ (cf. Remark 2). By careful inspection of Figure 6 one notices that the value of K may well remain constant over a range of thicknesses. In reality, the change in mode is not observable because it always happens through a double eigenvalue. So, when we use the term slope, we mean the slope of bands.

Conclusions and Future Work

We note that it has been highly advantageous to approach this problem using two different numerical discretizations. Our numerical results are in excellent agreement with the theoretical results, when available. In addition, we also get interesting results in the areas where the theory is still lacking. For the function $t \mapsto K_t$, similar techniques that have been used for the parabolic case (see [7]) could be used to cover the hyperbolic and elliptic cases also.

However, we expect the elliptic shell to be the most subtle case to analyse. Finally, the possible occurrence of numerical locking phenomena should be deeply investigated. Indeed, there is no rigorous analysis for this feature and will be addressed in future work.

References

1. E. Artioli, P.L. Gould and E. Viola. A Differential Quadrature method solution for shear-deformable shells of revolution. *Engineering Structures*, 2005, 27(13):1879-1892.
2. E. Artioli, L. Beirão da Veiga, H. Hakula and C. Lovadina, Free vibrations for some Koiter shells of revolution, submitted to *Appl. Math. Letters*.
3. E. Artioli, E. Viola. Free Vibration Analysis of Spherical Caps using a G.D.Q. Numerical Solution. *ASME Journal of Pressure Vessel Technology*, 2006, 128(3):370-378.
4. K-J. Bathe, D. Chapelle and P-S. Lee. A shell problem 'highly sensitive' to thickness changes. *Int. J. for Num. Meth. in Engrg.* 2003; 57:1039-1052.
5. L. Beirão da Veiga and C. Lovadina. An Interpolation Theory approach to Shell Eigenvalue Problems. To appear.
6. L. Beirão da Veiga and C. Lovadina. Asymptotics of Shell Eigenvalue Problems. *C.R. Acad. Sci. Paris.* 2006; 9:707-710.
7. L. Beirão da Veiga, H. Hakula and J. Pitkäranta. Asymptotic and numerical analysis of the eigenvalue problem for a clamped cylindrical shell. To appear.
8. N. Bellomo. Nonlinear models and problems in applied sciences from differential quadrature to generalized collocation methods, *Math. Comput. Modell.*, 1997, 26(4):13-34.
9. J. Bergh and J. Löfstrom. *Interpolation Spaces: an introduction*, Springer-Verlag, 1976.
10. C.W. Bert and M. Malik. Differential quadrature method in computational mechanics: a review, *Transactions of the American Society of Mechanical Engineers*, 1996, 49:1-28.
11. D. Chapelle and K.J. Bathe. Fundamental considerations for the finite element analysis of shell structures. *Comput. & Structures*, 1998; 66:19-36.
12. D. Chapelle and K.J. Bathe. *The Finite Element Analysis of Shells*, Springer-Verlag, 2003.
13. P.G. Ciarlet. *Introduction to Linear Shell Theory*, Series in Applied Mathematics, Gauthier-Villars, 1998.
14. M. Do Carmo. *Differential Geometry of Curves and Surfaces*. Prentice Hall, 1976.
15. C. Mardare. The Generalized Membrane Problem for Linearly Elastic Shells with Hyperbolic of Parabolic Middle Surface. *Journal of Elasticity*, 1998; 51:145-165.
16. H. Triebel. *Theory of Function Spaces II*, Birkhäuser, Basel, 1992.
17. P.L. Gould. *Analysis of Shells and Plates*, Prentice Hall, Upper Saddle River, NJ, 1999.
18. E. Sanchez-Palencia, *Statique et dynamique des coques minces. I. Cas de flexion pure non inhibée*, *C. R. Acad. Sci. Paris, Série I* **309** (1989) 411–417.
19. E. Sanchez-Palencia, *Statique et dynamique des coques minces. II. Cas de flexion pure inhibée - Approximation membranaire*, *C. R. Acad. Sci. Paris, série I*, **309** (1989) 531–537.
20. E. Sanchez-Palencia, Asymptotic and spectral properties of a class of singular-stiff problems, *J. Math. Pures Appl.* **71** (1992) 379–406.
21. W. Soedel. *Shells*, *Encyclopedia of Vibration*, Elsevier, 2001.
22. B. Szabo and I. Babuska. *Finite Element Method*, Wiley, 1991.
23. E. Viola, E. Artioli. The G. D. Q. method for the harmonic dynamic analysis of rotational shell structural elements. *Structural Engineering and Mechanics*, 2004, 17(6):789-817.

4 Appendix – The “monster” shell

In this Appendix we consider the following particular problem

- “Monster” shell (*Positive Gaussian curvature*). We choose (see Section 1.1, and also Figure 2(d))

$$\alpha = 0, \quad \beta = H = \frac{5}{\pi} \sin(2\pi/5), \quad f(x) = \sqrt{\frac{25}{\pi^2} - x^2}. \quad (29)$$

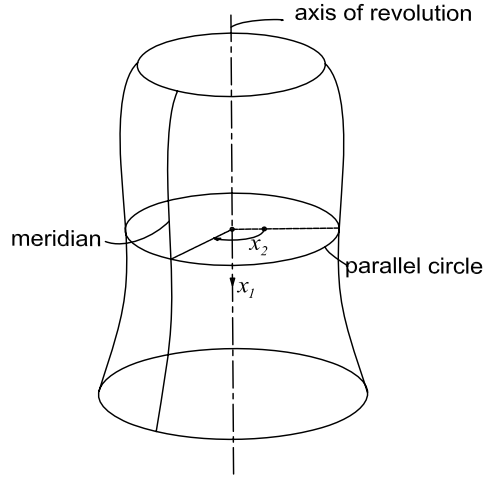


Fig. 1: Shell of revolution geometry and curvilinear coordinates over midsurface

The monster shell is clamped at $x_1 = 0$ and free at $x_1 = \frac{5}{\pi} \sin(2\pi/5)$. We consider also this additional case because of its peculiar asymptotic behaviour, as far as the corresponding source problem is concerned (see [4]).

We have performed the same numerical experiments as above also on the monster shell. The results are shown in Figures 7, 8 and 9. In this case the collocation method was not reliable for very small values of t and therefore only partial results are shown.

Some observations are immediate. The slope of $t \mapsto \omega_t^2$ is no longer easily recognizable, as a fluctuating behaviour is exhibited. Nor the limit value of $t \mapsto R(t, \mathbf{u}_t)$, if any, is clearly deducible. One may guess that $\lim_{t \rightarrow 0} R(t, \mathbf{u}_t) = 1$, which is also compatible with significant bending dominated regions for “small” but finite thicknesses (cf. Figure 5(d)).

Therefore, we may conclude that also for the vibration problem this example illustrates that our results are by no means exhaustive and a lot of work both in theory and numerical experiments remains to be done.

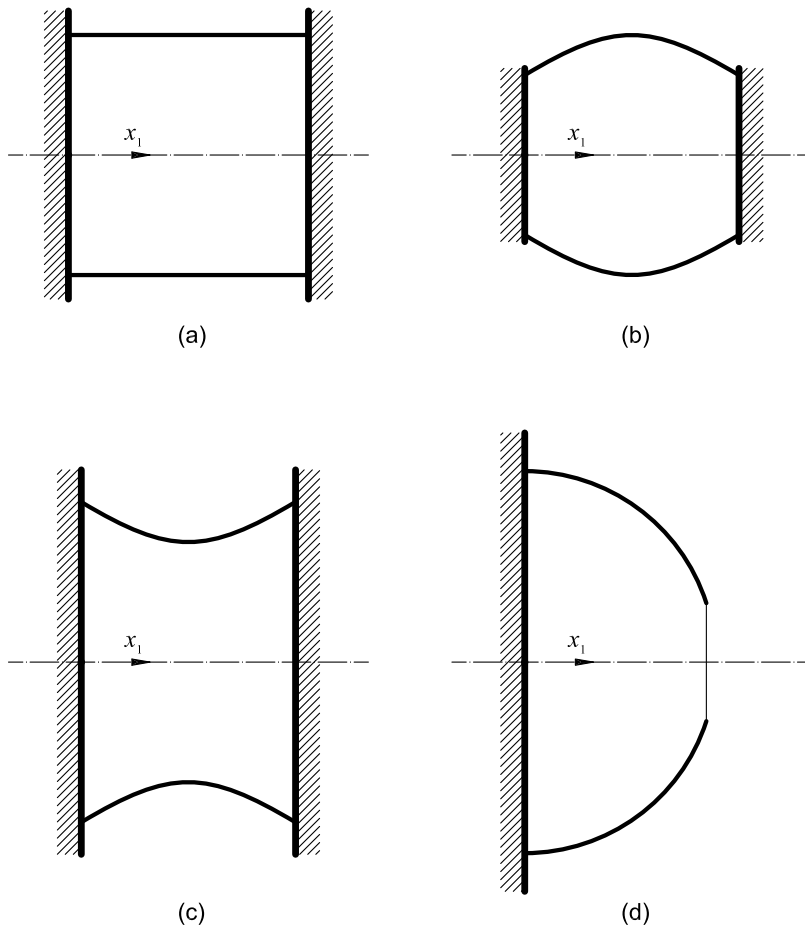


Fig. 2: Cross sections of analyzed shells: (a) parabolic cylinder (e) elliptic cylinder (c) hyperbolic cylinder (d) "monster" shell

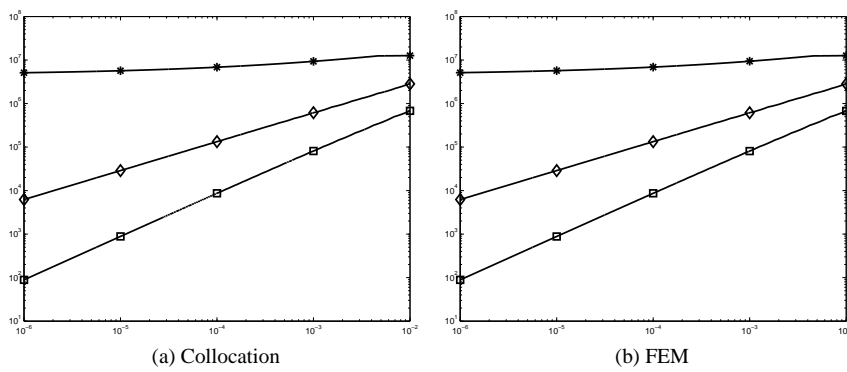
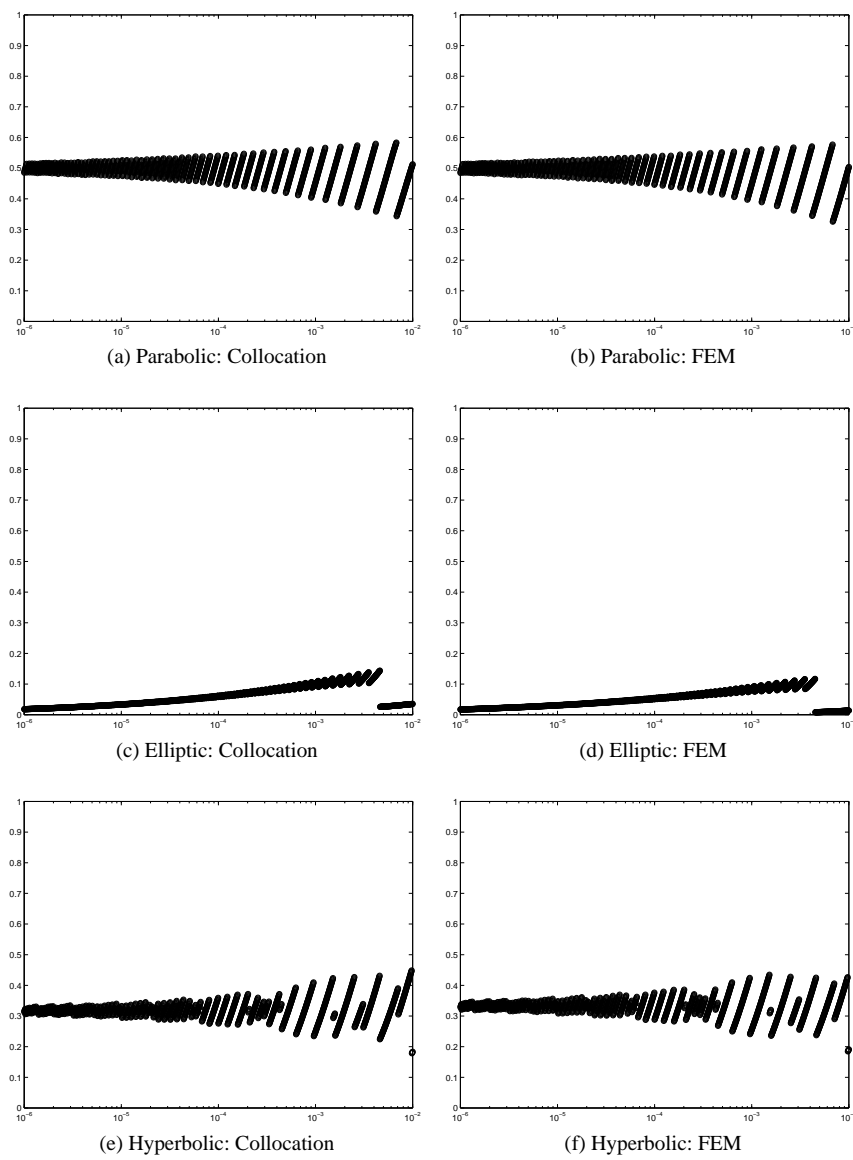
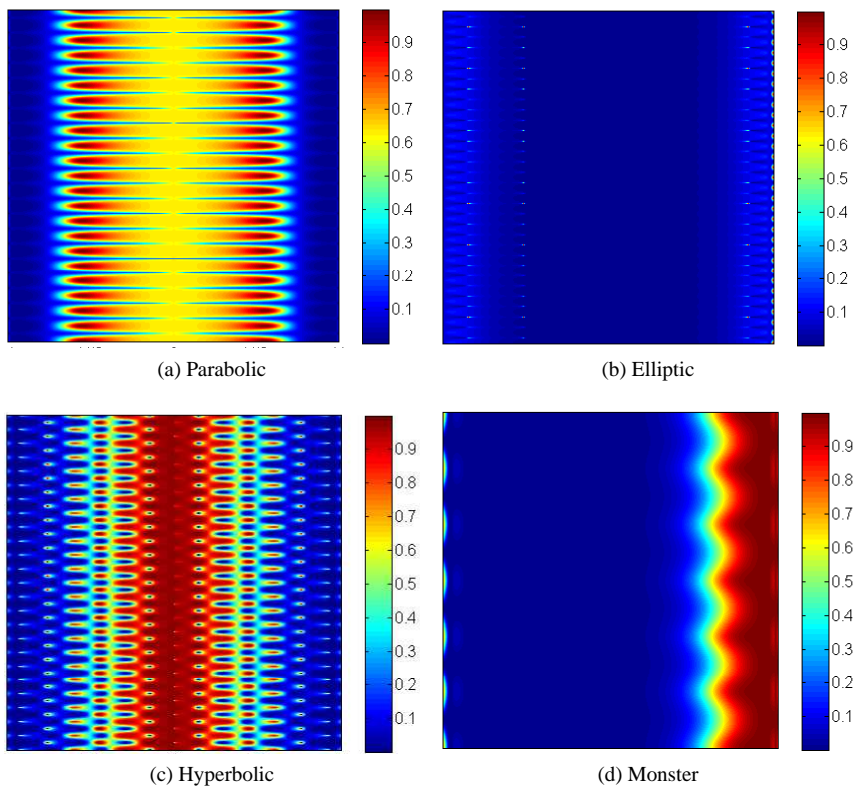


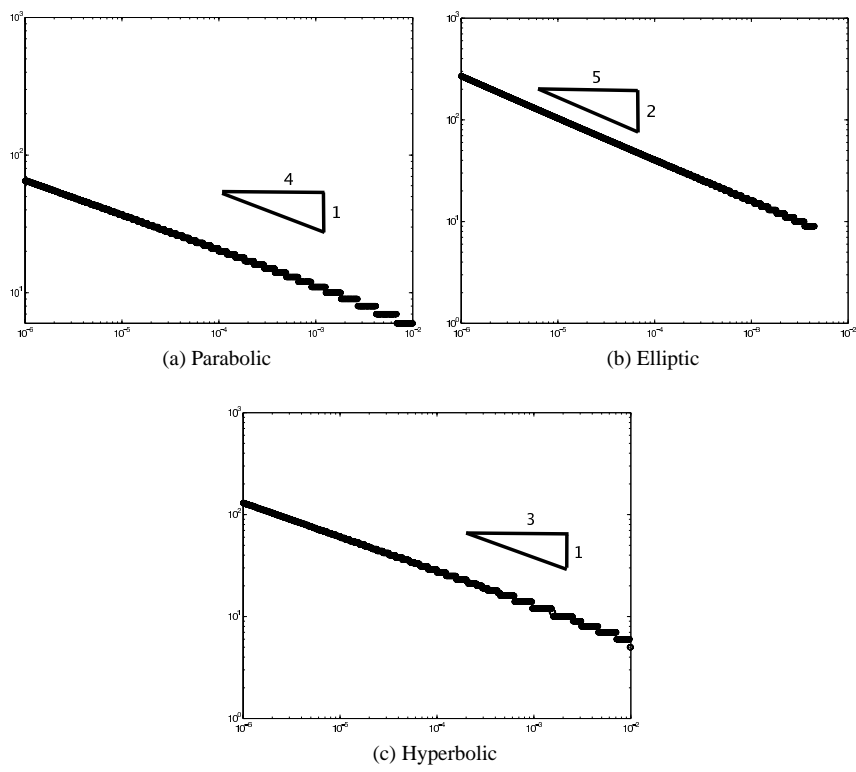
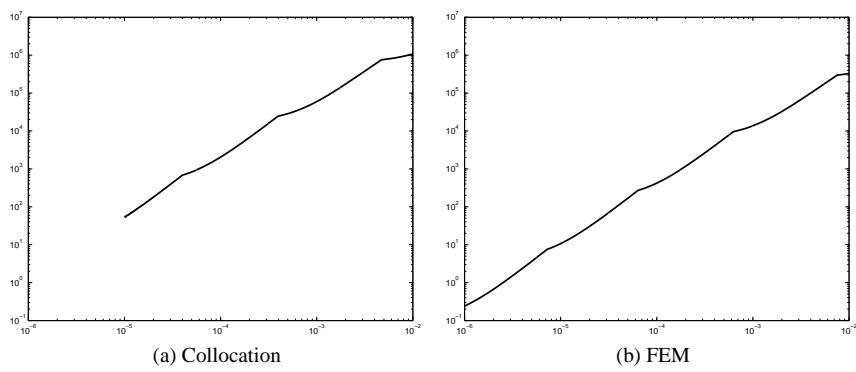
Fig. 3: $t \mapsto \omega_t^2$; Symbols: \square – Parabolic, $*$ – Elliptic, \diamond – Hyperbolic.

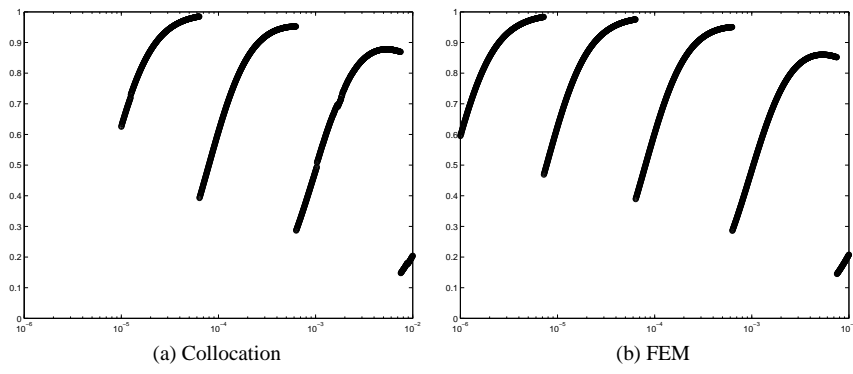
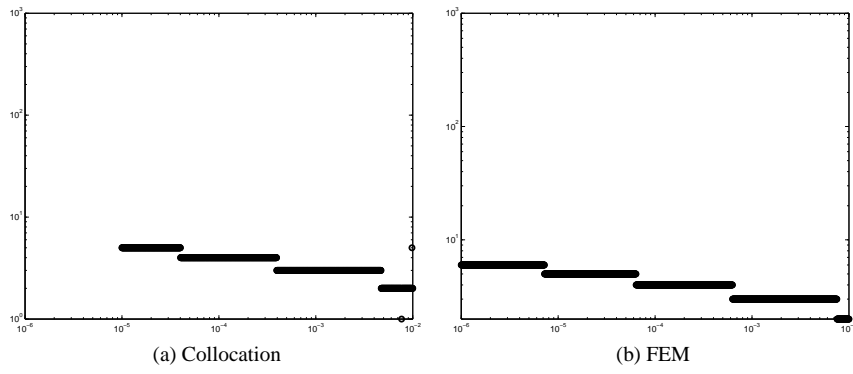
Fig. 4: $t \mapsto R(t, \mathbf{u}_t)$



Here we give the ratio between bending strain vs total strain energy density over the 2D -domain $[-1, 1] \times [0, \pi]$ (One half of the shell of revolution is unfolded onto the plane.). The red regions exhibit most bending.

Fig. 5: Plot of the ratio between bending strain vs total strain energy density: $t = 10^{-3}$.

Fig. 6: $t \mapsto K_t$.Fig. 7: $t \mapsto \omega_t^2$; Monster shell.

Fig. 8: $t \mapsto R(t, \mathbf{u}_t)$; Monster shell.Fig. 9: $t \mapsto K_t$; Monster shell.